Available online at www.sciencedirect.com

SCIENCE DIRECT®

ELSEVIER

Palaeogeography, Palaeoclimatology, Palaeoecology 227 (2005) 18–30

PALAEO

www.elsevier.com/locate/palaeo

Concretionary methane-seep carbonates and associated microbial communities in Black Sea sediments

J. Reitner [a,*], J. Peckmann [b], M. Blumenberg [c], W. Michaelis [c], A. Reimer [a], V. Thiel [a]

[a] *Geowissenschaftliches Zentrum der Universität Göttingen, Goldschmidtstraße 3, 37077 Göttingen, Germany*
[b] *Forschungszentrum Ozeanränder, Universität Bremen, Postfach 330440, 28334 Bremen, Germany*
[c] *Institut für Biogeochemie und Meereschemie, Universität Hamburg, Bundesstraße 55, 20146 Hamburg, Germany*

Received 11 June 2004; received in revised form 24 September 2004; accepted 11 April 2005

Abstract

Gas seeps in the euxinic northwestern Black Sea provide an excellent opportunity to study anaerobic, methane-based ecosystems with minimum interference from oxygen-dependent processes. An integrated approach using fluorescence- and electron microscopy, fluorescence in situ hybridization, lipid biomarkers, stable isotopes ($\delta^{13}C$), and petrography revealed insight into the anatomy of concretionary methane-derived carbonates currently forming within the sediment around seeps. Some of the carbonate concretions have been found to be surrounded by microbial mats. The mats harbour colonies of sulphate-reducing bacteria (DSS-group), and archaea (ANME-1), putative players in the anaerobic oxidation of methane. Isotopically-depleted lipid biomarkers indicate an uptake of methane carbon into the biomass of the mat biota. Microbial metabolism sustains the precipitation of concretionary carbonates, significantly depleted in ^{13}C. The concretions consist of rectangularly orientated, rod- to dumbbell-shaped crystal aggregates made of fibrous high Mg-calcite. The sulphate-reducing bacteria exhibit intracellular storage inclusions, and magnetosomes with greigite (Fe_3S_4), indicating that iron cycling is involved in the metabolism of the microbial population. Transfer of Fe^{3+} into the cells is apparently mediated by abundant extracellular vesicles resembling known bacterial siderophore vesicles (marinobactine) in size (20 to 100 nm) and structure.

Keywords: Seeps; Methane; Archaea; Magnetotactic bacteria; Carbonate concretions; Greigite; Black Sea

1. Introduction

Most methane seeping upward in the marine sedimentary column is intercepted biologically by a process known as anaerobic oxidation of methane (AOM; see Valentine, 2002 and Hinrichs and Boetius, 2003 for recent reviews). It is now generally

* Corresponding author. Tel.: +49 551 397950; fax: +49 551 397918.
E-mail address: jreitne@gwdg.de (J. Reitner).

0031-0182
doi:10.1016/j.palaeo.2005.04.033

accepted that AOM is mediated by consortia of methane-oxidizing archaea and sulphate-reducing bacteria (SRB), although the exact mechanism(s) are not well understood and metabolic intermediates are still not known. According to the overall reaction

$$CH_4 + SO_4^{2-} \rightarrow HCO_3^- + HS^- + H_2O.$$

AOM increases carbonate alkalinity, resulting in ^{13}C-depleted limestones which are typically found as geological manifestations of contemporary and ancient methane seepage (Ritger et al., 1987; Bohrmann et al., 1998; Greinert et al., 2001; Peckmann et al., 2001; Aloisi et al., 2002; Campbell et al., 2002; Lein et al., 2002; Stadnitskaia et al., 2003; Peckmann and Thiel, 2004).

In the northwestern Black Sea, methane seepage frequently occurs on the shelf/slope southwest of the Crimean Peninsula (Egorov et al., 1998). Within anoxic bottom waters, ^{13}C-depleted, methane-derived carbonates ($\delta^{13}C < -20‰$) are typically found at the seep locations. Carbonate crusts and concretions forming within the sediment are abundant in regimes of diffusely ascending methane fluxes. At sites of intense gas discharge, these precipitates may grow into the anoxic water column, forming tower-like buildups up to several metres in height (Ivanov et al., 1991; Luth et al., 1999; Peckmann et al., 2001; Lein et al., 2002; Michaelis et al., 2002).

Microbial mats are typically attached to the carbonate towers. Their microbiology and physiology has previously been studied (Pimenov et al., 1997; Michaelis et al., 2002; Tourova et al., 2002). Laboratory experiments with ^{14}C- and ^{35}S-labelled substrates indicated that the mats have the capacity to perform AOM and sulphate reduction (Pimenov et al., 1997; Michaelis et al., 2002). A concurrent transfer of methane carbon into the biomass of archaea and SRB was inferred from the occurrence of specific lipid biomarkers highly depleted in ^{13}C (Thiel et al., 2001a; Michaelis et al., 2002; Blumenberg et al., 2004). Microscopy and culture independent molecular work identified archaea of the ANME-1 and ANME-2 (anaerobic methane oxidizers) clusters, SRB of the *Desulfosarcina/Desulfococcus* (DSS) group, and previously unknown Crenarchaeota in mats covering the carbonate buildups (Pimenov et al., 1997; Michaelis et al., 2002; Tourova et al., 2002; Blumenberg et al., 2004). Recently, Krüger et al. (2003) discovered a conspicuous nickel protein, similar to the terminal enzyme of archaeal methanogenesis, and most likely responsible for the anaerobic oxidation of methane, in mats sampled from the towers described by Michaelis et al. (2002). However, our knowledge of the community structures and the biogeochemical pathways operating in different facies of the methane-fuelled Black Sea ecosystem is still fragmentary. We here report on the anatomy of concretionary methane-derived carbonates and associated microorganisms, using an integrated approach to provide new insights into the microbial ecology of this unique, methane-dominated environment.

2. Materials and methods

Samples were taken at seeps on the lower Crimean shelf during a German–Russian–Ukrainian joint expedition (GHOSTDABS) in 2001 (Fig. 1). For sampling, a TV-guided grab was used from aboard the Russian R/V "Professor Logachev". The samples described here were taken at 235 m depth (LOGA 01/11; 44°46.510′ N, 31°59.570′ E). Samples were frozen immediately after sampling, and aliquots were fixed with 4% buffered formol, stored in 70% ethanol or in 50% phosphate buffered saline (PBS). Samples for transmission electron microscopy (TEM), conventional scanning electron microscopy (SEM), and field emission SEM (FE-SEM) were fixed with 4% buffered glutardialdehyde and post fixed with 2% OsO_4. Thin sections of microbial mats were cut using a Leica hardpart microtome (for details, see Reitner, 1993; Hoffmann et al., 2003). Image stacks with a *Z*-spacing of 0.5 or 0.25 μm were obtained by using a piezomover (Physik Instrumente GmbH and Co, Waldbronn) attached to a "Plan-Apochromat" ×63-objective (Zeiss, NA=1.4) of a Zeiss Axioplan microscope. Image processing was carried out by using the Metamorph® Imaging software (Universal Imaging Corporation, West Chester, PA) and the EPRTM deconvolution software (Scanalytics, Billerica, MA) (Manz et al., 2000). Paraffin sections of decalcified samples were stained with various histochemicals, namely toluidine blue O for carbohydrate detection, 16S rRNA oligonucleotide probes for fluorescence in situ hybridisation (FISH), Nile blue A for polyhy-

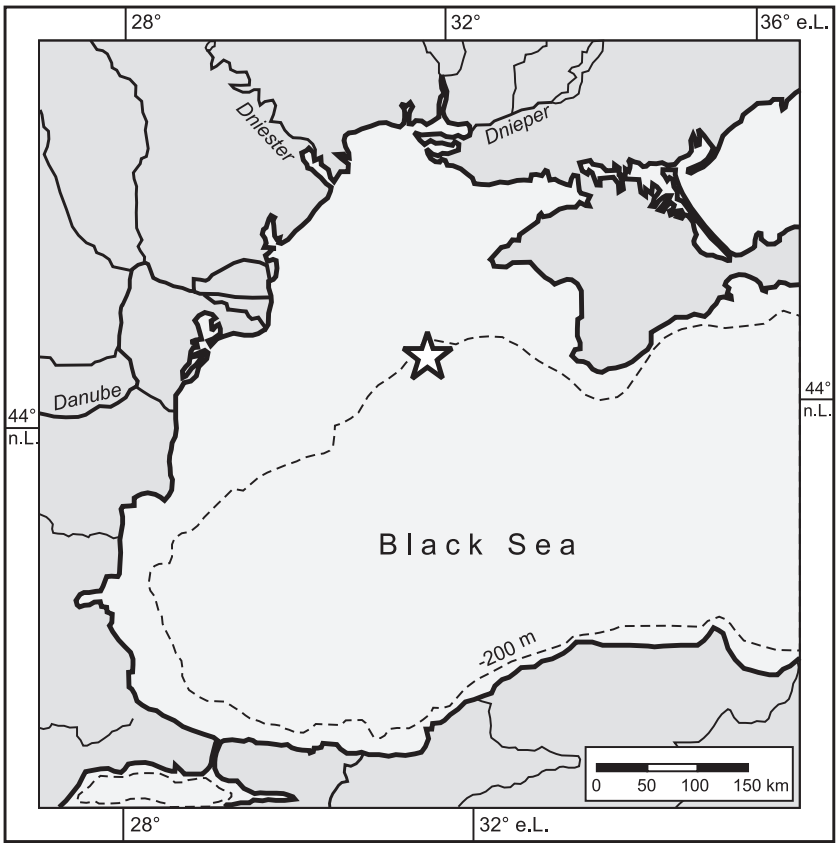

Fig. 1. Location of the working area.

droxyalkanoate (PHA) detection (Romeis, 1989), and DAPI (4′,6-diamidino-2-phenylindole) for DNA and RNA detection (for details, see Romeis, 1989; Manz et al., 2000; Hoffmann et al., 2003).

Prior to FISH, the samples were stained with DAPI to control the cell numbers and vitality of the microbial communities. The DAPI control-stain is important to avoid misinterpretations and to recognise non-specific binding artefacts of the oligonucleotide probes. Each section was hybridised with two differently labeled oligonucleotide probes.

The probes were purchased 5′-labeled with the indocarbocyanine dye Cy3 (Amersham Pharmacia Biotech) and Oregon Green (Molecular Probes) from Biometra (Göttingen, Germany), and were stored in TE buffer (10 nM Tris/1 mM EDTA, pH 7.5) at −20 °C. In order to minimize mismatching of the oligonucleotide probes, several sections of each mat sample were hybridised using varied buffer stringencies (formamide concentrations) from 35% to 60% at set hybridisation and wash temperatures. When using bacterial together with archaeal probes, best results were obtained with a hybridisation solution of 40% stringency. This solution was prepared by mixing 400 μl doubly distilled water with 400 μl formamide, 180 μl 5 M NaCl, 20 μl 1 M Tris (pH 8), and 1 μl 10% SDS. Prewarmed hybridisation solution was mixed with fluorescently labeled oligonucleotide (1 ng/μl of hybridisation solution).

The following oligonucleotide probes were used: EUB338 (Amann et al., 1990a), ARCH915 (Amann et al., 1990b), DSS658 (Manz et al., 1998), ANME-1 (Hinrichs et al., 1999), EelMS932-ANME-2 (Boetius et al., 2000). Glutardialdehyde-fixed samples were dried with Peldri II (Pelco, USA) and HMDS (hexamethyldisilazane; Polysciences, USA) to avoid drying artefacts. Peldri II and HMDS are chemical

alternatives to critical point drying. Details of the very simple procedure are described in Brown (1993).

Uncoated samples were investigated by FE-SEM using a LEO 1530 Gemini instrument at less than 1 kV. Energy dispersive X-ray spectrometry (EDX) was performed on the same instrument using carbon-coated samples, and applying a gun voltage of 13 kV. In order to avoid dehydration artefacts and collapse of organic structures, some samples were investigated fully hydrated using an Oxford-Cryosystem attached to the FE-SEM. TEM investigations were carried out with a Zeiss EM 10 instrument at 60 to 80 kV. Carbonate samples for stable carbon isotope analysis were prepared using a hand-held microdrill. CO_2 was generated by reaction with orthophosphoric acid and analysed with a Finnigan MAT 251 mass spectrometer. The $\delta^{13}C$ results are reported relative to the V-PDB standard (precision of values is $\pm 0.05‰$) and appropriate correction factors were applied.

Lipid biomarkers were extracted from the concretional carbonate and an associated microbial mat. Background sediment was analysed as a reference. A detailed description of the analytical procedure is given in Thiel et al. (2001a). Briefly, the thawed samples were decalcified using HCl. Lipids were saponified by refluxing in 6% KOH/methanol, and partitioned in CH_2Cl_2. Fractions were obtained by column chromatography, and analyzed by GC–MS. Compound specific isotope measurements were performed using gas chromatography–combustion–isotope ratio mass spectrometry (GC–C–IRMS). The stable carbon isotope compositions are given as $\delta^{13}C$-values vs. V-PDB ($s = < 1.0‰$.).

3. Results and discussion

3.1. Carbonates

Close to the Dniepr Canyon, in anoxic waters at depths between 200 and 400 m, methane seepage sustains the formation of authigenic carbonates within the sediment. Two types of precipitates have been sampled with the TV-guided grab. The first type consists of porous plates of lithified and semi-lithified sediments (Fig. 2A). The plates are cemented by automicritic (sensu Reitner et al., 1995), high Mg-calcite with up to 13 mol% $MgCO_3$. The carbonate matrix contains only a few coccoliths, little silt, and sparse allochthonous carbonate components. Methane microseepage is thought to have induced the formation of large, elongated (stromatactoid) and spherical voids, with the latter probably marking the locations of former gas bubbles (Fig. 2B). These structures resemble the ‘birds eye’ structures often observed in fossil tidal flat carbonates. Due to rapid lithification, the cavities are not compacted. Some of them are cemented by granular high Mg-calcite, and most internal surfaces are covered by biofilms (Fig. 2C). The automicritic carbonate shows $\delta^{13}C$ values below $-20‰$ V-PDB (Fig. 2B), indicating that a significant portion of the carbonate carbon is derived from methane.

The second type of carbonate forming within the sediments comprises lenticular concretions. They consist of high Mg-calcite and range in size from several centimetres to a few decimetres. Several concretions are commonly interconnected and then form larger aggregates (Fig. 2D). A higher content of background sediment is present in the core of some concretions (Fig. 2E). Outer and inner surfaces of several concretions were found to be coated by grey or pink-coloured microbial mats (Fig. 2D). Due to inclusions of organic matter, the concretionary carbonates show a specific autofluorescence, different from that of the surrounding sediment (Fig. 2F). The lenticular concretions consist of ca. 100 μm sized, elongated rod- to dumbbell-shaped crystal aggregates of fibrous calcite (Fig. 3A–D). Toluidine blue O staining reveals dense populations of microorganisms surrounding the crystallites, indicating that microbes mediated the formation of these precipitates (Fig. 3D). The aggregates show a near-rectangular orientation (Fig. 3A) which is also inherent in the orientation of abundant twin crystals (Fig. 3C). As AOM triggers carbonate precipitation through an increase in carbonate alkalinity, we further suggest that the regular fabric of the precipitates may be controlled by the meta-structures of organic matrices provided by excreted EPS (extracellular polymeric substances).

The high Mg-calcite yielded a $\delta^{13}C$ value of $-28‰$ V-PDB, indicating that a significant portion of the carbonate carbon derives from AOM. In organic extracts of bulk carbonate and a microbial mat

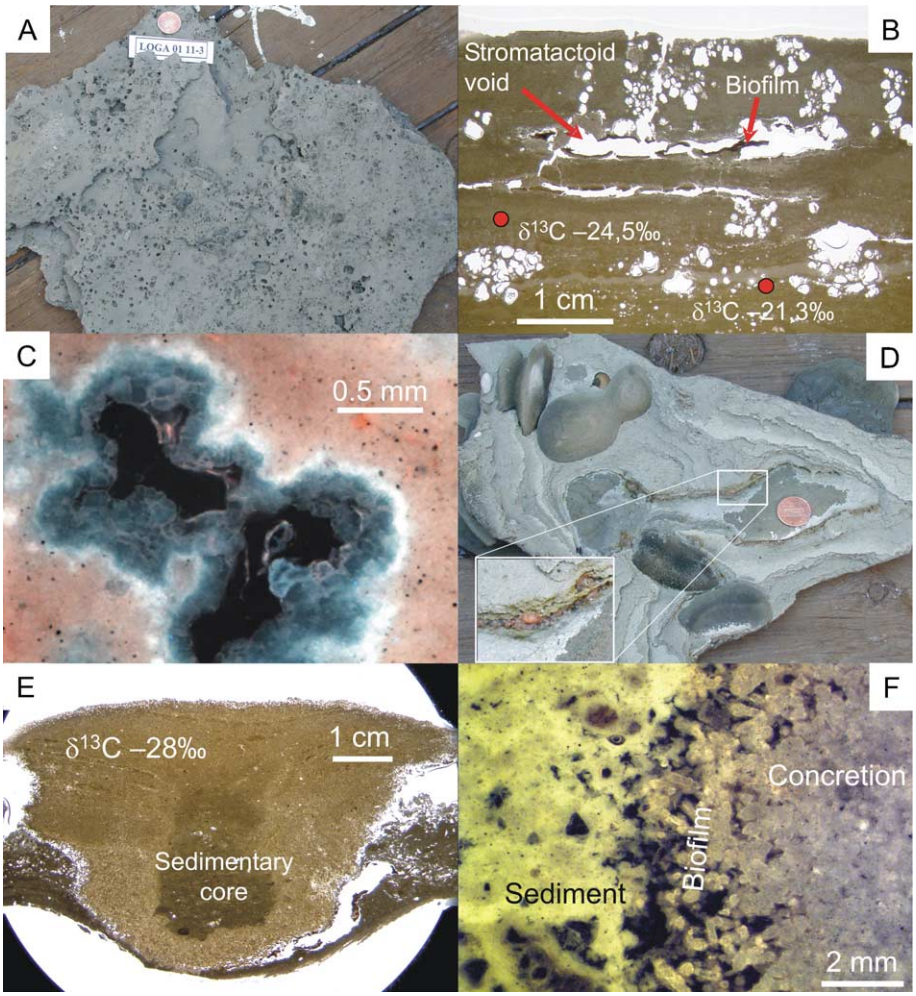

Fig. 2. Morphology and fabrics of seepage-related carbonates. (A) Cemented carbonate sediment with abundant cavities eventually representing former gas bubbles. Due to early cementation the carbonate crust has not been affected by compaction. The coin is 19 mm in diameter. (B) Thin section of the crust shown in (A) (air dried sample), showing voids within the carbonate that formed by gas seepage. Internal surfaces of the cavities are commonly covered with biofilms. (C) UV-fluorescence micrograph showing bird's eye-like voids within the concretion's matrix formed of high Mg-calcite. The strongly fluorescent rim at the contact between sediment and cement may result from organic matter derived from a mineralized biofilm. The coin is 19 mm in diameter. (D) Lenticular carbonate concretions embedded in lithified, well-bedded background sediments. Note that the lenticular concretions in the upper left are orientated sub-vertical to bedding. Insert shows a thick microbial mat surrounding the carbonate concretion. (E) Thin section of a carbonate concretion showing that background sediment predominates in the central part of the concretion, whereas the outer regions consist of virtually pure authigenic carbonate. Assuming a radial growth mode, this suggests that the initial stage of concretion formation involves the cementation of sediment, whereas further growth is characterized by displacement of the surrounding material. (F). Lenticular concretions are commonly surrounded by biofilms. The fluorescence micrograph using a Zeiss no. 487709 fluorescence filter (resulting in a green fluorescence) indicates enrichment of organic matter within the enclosing sediment as well as in the peripheral, newly forming portions of the concretion.

sample, we found isoprene-based membrane lipids derived from Archaea, and straight-chain carbon skeletons of putative bacterial origin. Strong depletions in ^{13}C, with $\delta^{13}C$ values in the range of −70‰ to −100‰ (Table 1) allow methane-related compounds to be differentiated from allochthonous marine lipids ($\delta^{13}C \sim -20‰$ to −30‰), and imply that methane carbon is transferred into the biomass of the source

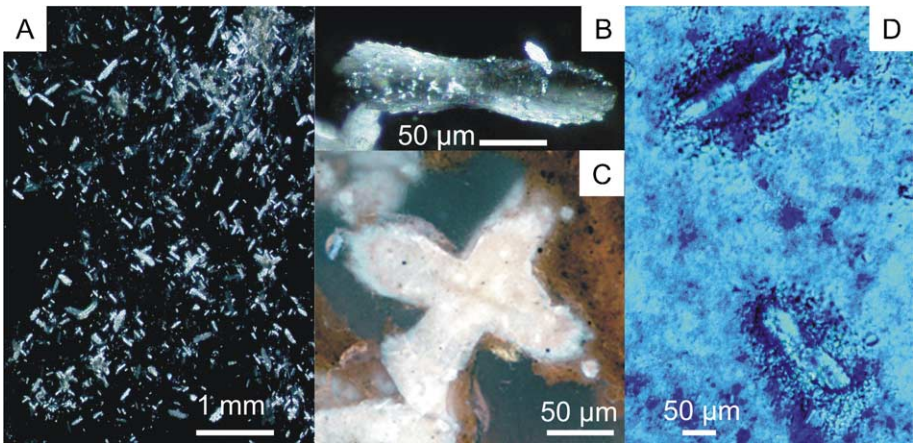

Fig. 3. Hardpart-microtome sections of the microbial mat surrounding the concretional carbonate shown in Fig. 2D. (A) Elongated high Mg-calcite crystallites (bluish) show a near-rectangular orientation, possibly controlled by the internal meta-structure of microbial EPS (cross-polarized light). (B) The individual crystal aggregates consist of high Mg-calcite and exhibit a rod- to dumbbell-like habit (cross-polarized light). (C) A twin crystal aggregate which appears to inherit the near-rectangular orientation of the crystal aggregates shown in A (UV autofluorescence micrograph). Using UV-fluorescence (UV-high performance narrow-band filter 487701 Zeiss) the Mg-calcites exhibit a very strong bright-blue fluorescence. Using the wide band pass filter 487709, the same phase shows no intense autofluorescence (see Fig. 2F). (D) Toluidine blue O staining reveals dense microbial populations surrounding each crystallite. This suggests that microbial metabolism triggers carbonate precipitation, likely due to an increase of alkalinity upon AOM.

biota. Similar ^{13}C-depleted biomarkers have been observed in carbonate crusts, towers, and associated mats from nearby sites (Thiel et al., 2001a; Michaelis et al., 2002; Blumenberg et al., 2004), in carbonate crusts from the Sorokin Trough (NE′ Black Sea, Stadnitskaia et al., 2003), and in other methane-rich environments (Hinrichs et al., 1999; Elvert et al., 2000; Pancost and Sinninghe Damsté, 2003). Due to their structures and ^{13}C-depletions, these compounds have been consistently related to contributions from methane-consuming archaea and metabolically associated SRB.

3.2. Microbiology

TEM analyses of fixed mat samples revealed abundant cylinder-shaped microorganisms having external sheaths (Fig. 4A). The sheaths seem to consist of a resistant biopolymer, as empty sheaths tend to become enriched and make up a major portion of the mats

Table 1
δ^{13}C values [‰ V-PDB] and sources of selected biomarkers from the concretional carbonates

Compound	Source[1]	Bulk concretion LOGA 01/11-4; 104	Microbial mat LOGA01/11-4; 105
PMI	Archaea[2]	−86.4	−89.5
Archaeol	Archaea[3]	−95.6	−102.7
n-Tricos-10-ene (*n*-C_{23}^{10})	Unknown (SRB?)[4]	−85.1	−84.8
ai-C_{15}-Diether	SRB[5]	−78.0	−59.1*
Phytol	Algae, higher plants	−33.4	−32.4
n-Hentriacontane (*n*-C_{31})	Algae, higher plants	−30.4	−30.4
24-Methylcholesta-5,22-dien-3β-ol	Mainly algae	−30.4	−30.1

The $\delta^{13}C_{methane}$ values in the study area range from −62.4‰ to −68.3‰ (Michaelis et al., 2002). [1] 'Source' column denotes most likely biological origin for AOM-related biomarkers according to: [2] Elvert et al. (2000), [3] Hinrichs et al. (1999), [4] Thiel et al. (2001b), [5] Pancost et al. (2001). *=major coelution with a phytoplankton-derived sterol.

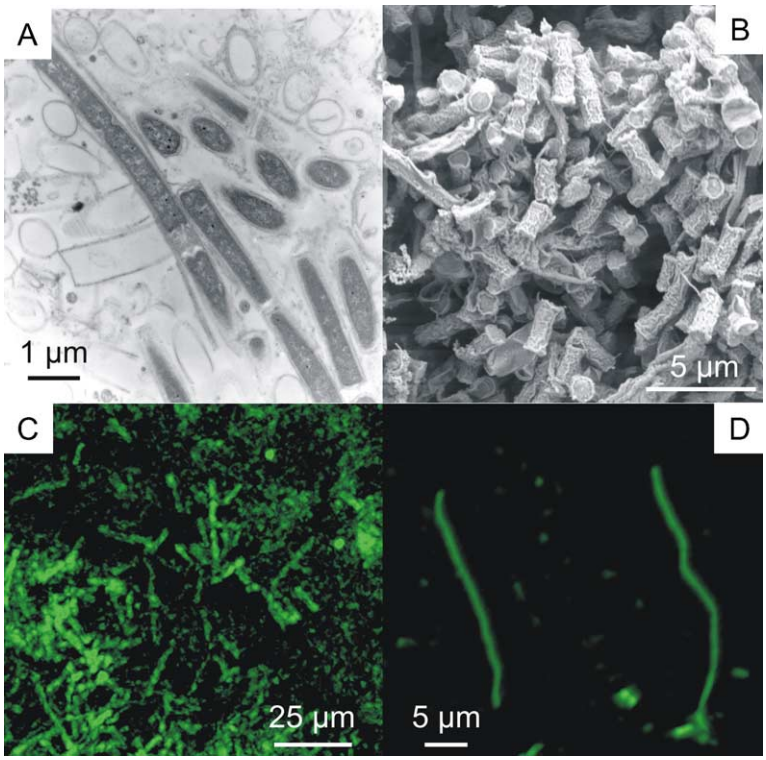

Fig. 4. ANME-1 archaea in the microbial mat surrounding concretional carbonate. (A) Cells of cylinder-shaped ANME-1 archaea may be arranged into chains, and are separated by distinct invaginations functioning as pull linkages. TEM micrograph. (B) Three-dimensional arrangement of cylinder-shaped ANME-1 sheaths. FE-SEM image of a native (unsputtered) Peldri II-dried sample. (C, D) Fluorescence images of thin sections treated with an oregon green labelled oligonucleotide probe specific for archaea of the ANME-1 cluster. The probe responds to cells with two distinct morphologies, i.e. shorter chains of cylinder-shaped cells (C), and very long filamentous forms (D).

(>80 vol.% in some sections, see Figs. 4A, 6A). In places, therefore, the microbial mats primarily consist of dead biomass by volume. The cylindrical, can-like shape of single cells can be visualised by FE-SEM (Fig. 4B). Single cells have a diameter between 0.6 and 1 µm, and are variable in length (mostly 2 to 3 µm). They form multicellular filaments in which the single cells are separated by distinct invaginations (Fig. 4A). FISH analyses of these samples revealed strong signals from archaea of the ANME-1 cluster (Fig. 4C), which has been previously related to AOM (Hinrichs et al., 1999). We assume that these ANME-1 archaea are identical to those reported from this seep area using microscopy (Pimenov et al., 1997), FISH (Michaelis et al., 2002; Blumenberg et al., 2004), and a 16S rRNA survey (Tourova et al., 2002). The ANME-1 probe also responded to extremely long multicellular chains, sometimes exceeding 100 µm in length (Fig. 4D). Such long filamentous forms were previously recognized microscopically by Pimenov et al. (1997), and interpreted as different growth stages of the shorter, cylinder-shaped microbes. ANME-1 archaea with a similar morphology were also visualized by FISH of microbial consortia from methane-rich sediments of the Eel River Basin (Orphan et al., 2002).

Some of the cylinder-shaped ANME-1 cells contain structures that resemble thick stacks of intracytoplasmic membranes (Fig. 5A, B). These stacks are similar to membrane assemblages found as the site of the C_1-metabolism in Type I and Type X aerobic methanotrophic bacteria (Fig. 5C). It is tempting to anticipate an analogous function of the membranous structures inside the ANME-1 cells, inasmuch because common gene coding for C_1-transfer enzymes has recently been found to exist among methanotrophic bacteria and methanogenic archaea (Chistoserdova et al., 1998). The presence of internal

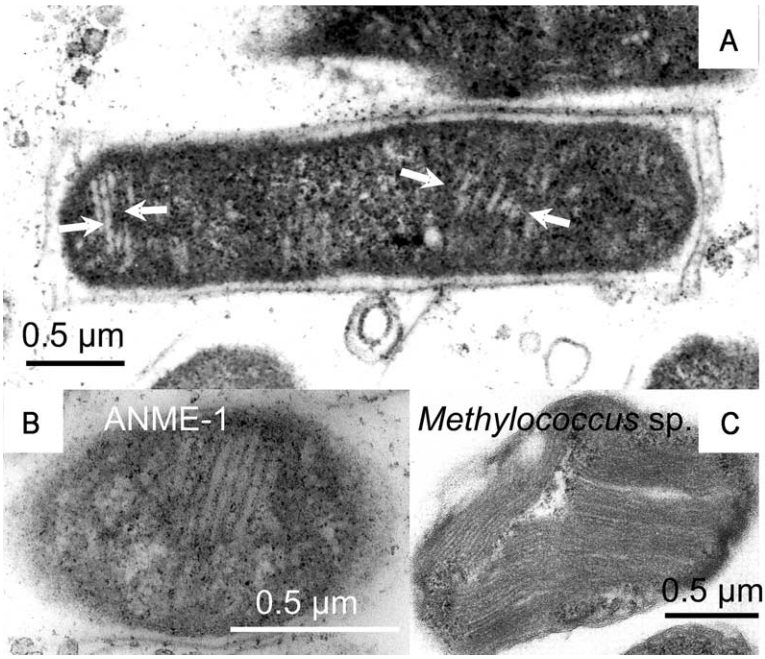

Fig. 5. Ultrastructure of ANME-1 cells. (A, B) Cylinder-shaped ANME-1 cell showing stacks of putative intracytoplasmic membranes (arrows). TEM micrograph. (C) Intracytoplasmic membranes in a methanotrophic, aerobic bacterium sampled from saline deep waters from the Äspö Hardrock Laboratory, southern Sweden. TEM micrograph.

membranes in a methanogenic Archaeon, *Methanobacterium thermoautotrophicum*, has been reported earlier, and a function of the membranes related to the methane metabolism was suggested (Zeikus and Wolfe, 1973). However, later on it was found that internal membranes in archaeal cells may be formed artifactually upon sample preparation using particular buffers and weak fixatives (Aldrich et al., 1987, and refs. therein). The stack-like structures seen in the Black Sea ANME-1 archaea differ strongly in ultrastructure from the putatively artifactual, concentric 'technikosomes', and the invaginations of the plasma-membranes observed by Aldrich et al. (1987) and Zeikus and Wolfe (1973). However, the phenomenon was observed only in part of the TEM sections studied. Further efforts are underway in our laboratory to validate the existence of internal membranes by employing different fixation procedures on newly collected ANME-1 archaea.

Among other yet unidentified microbiota, another component of the mat population are microbes forming large, localized colonies of some tens of micrometers in diameter (Fig. 6A). FISH analyses revealed a strong response to the DSS 658 probe, suggesting that the colony-building organisms are SRB belonging to the *Desulfosarcina/Desulfococcus* group (DSS, Fig. 6B). DSS have previously been reported as the predominant SRB in a microbial mat sampled from a near-by carbonate tower (Michaelis et al., 2002). However, these authors reported coccoid forms with an internal diameter of about 0.6 µm. The bacteria reported here show similar internal diameters (0.5 to 1 µm), but longitudinal cell sections reveal that they are vibrioform, with cell lengths of 3 µm and more (Fig. 6C). It is therefore unlikely that these bacteria belong to the same DSS-taxon as those described by Michaelis et al. (2002).

The concretion-associated SRB are typically found in association with ANME-1 archaea. The ANME-1 cells are most frequent close to the periphery of SRB-colonies (Fig. 6A). However, isolated, monospecific clusters of ANME-1 archaea have been observed as well. This may indicate that a spatial proximity to SRB is not required for the archaeal metabolism, but it may also represent a

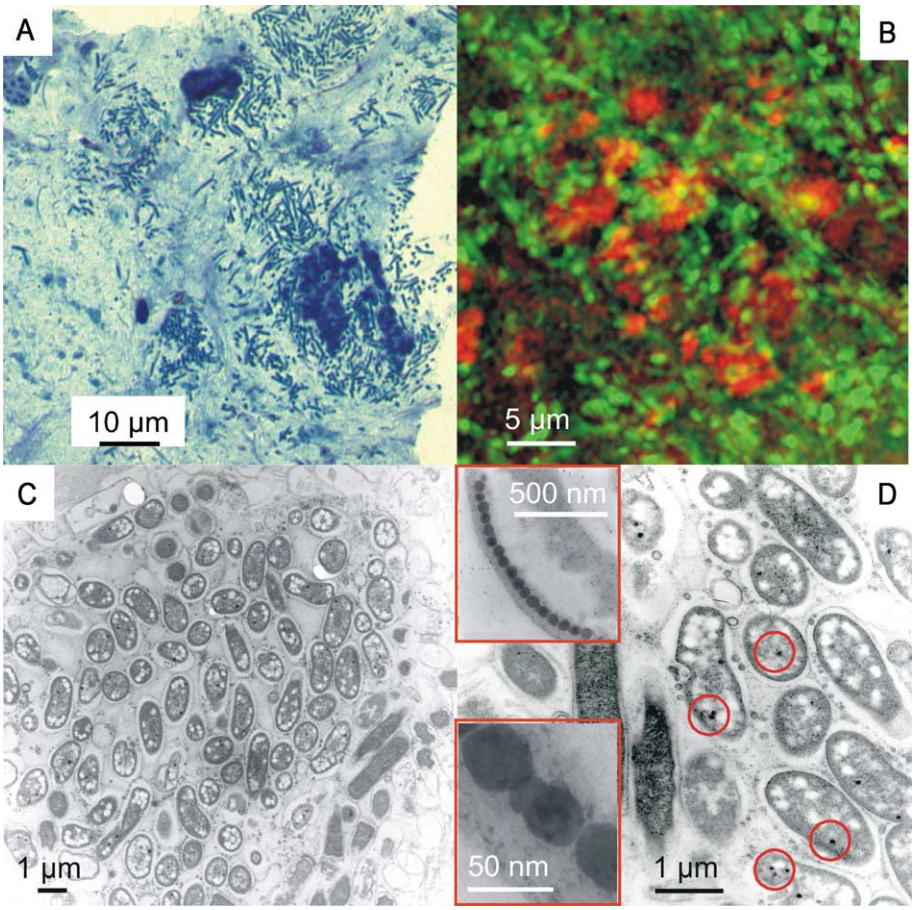

Fig. 6. Sulphate-reducing bacteria (SRB) in the microbial mat surrounding the carbonate concretions. (A) Spatial arrangement of ANME-1 archaea surrounding clusters of SRB (dense, dark blue clusters). Toluidine blue O stained semi-thin section. (B) Assemblage of ANME-1 archaea and SRB. Fluorescence micrograph (FISH) of a section stained with an oregon green labelled probe specific for ANME-1 archaea and a red-fluorescent (cy3) labelled probe specific for SRB of the *Desulfosarcina/Desulfococcus* group (DSS 658). (C) SRB colony. Longitudinal sections reveal a vibrioform cell morphology. PHA appear as bright inclusions within the cells. TEM micrograph. (D) Magnetosomes in the concretion-associated SRB. Greigite crystals appear as individual globules in perpendicular cell sections (circles). Only in longitudinal sections the chain-like-arrangement of greigite globules is evident (inserts). A blotchy, non-uniform diffraction contrast is a typical feature of the greigite crystals (insert, bottom). TEM micrographs.

preparation artefact due to marginal sectioning of some of the microbial aggregates.

3.3. Intracellular sulphides and PHA

A remarkable feature of the SRB is that they contain abundant droplets resembling storage inclusions of polyhydroxyalkanoates (PHA; Fig. 6C, D). The presence of PHA was corroborated by staining with the lipophilic dye Nile blue A, which caused a specific, bright yellow fluorescence of the PHA-containing inclusions (Zeiss no. 487709 wide-band pass filter, BP 450-490, LP 520). These results agree with the very recent discovery of PHA in members of the DSS-group, including *Desulfosarcina variabilis* and *Desulfococcus multivorans* (Hai et al., 2004). Longitudinal cell sections also reveal intracellular aggregates of crystallites showing a somewhat blotchy diffraction contrast in the TEM (Fig. 6D, inserts). By size (~30 to 80 nm in diameter) and arrangement (chains, clusters), they strongly resemble precipitates formed by the so-called magnetotactic bacteria (Pósfai

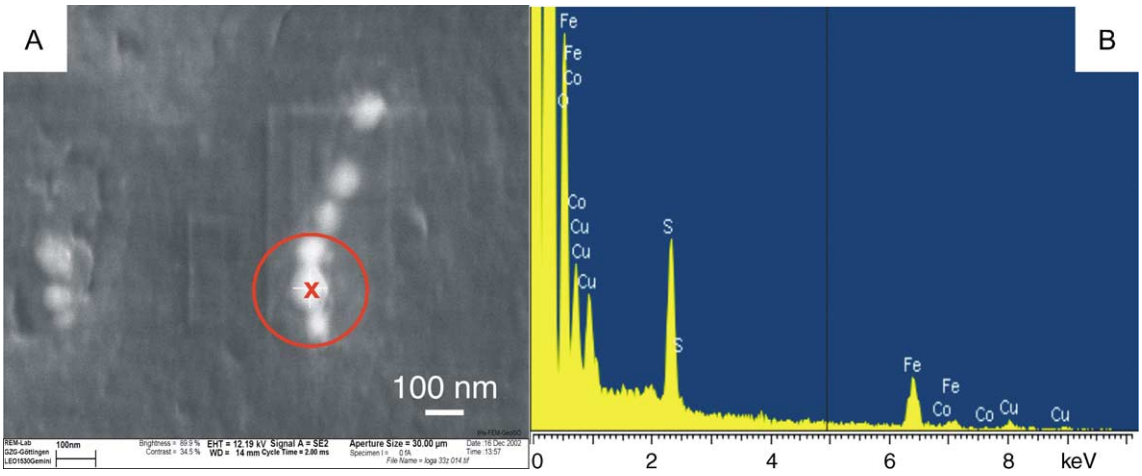

Fig. 7. Intracellular magnetosomes visualized by FE-SEM. The ferrimagnetic greigite crystals occur as distinct white spherules (A). 'x' marks the beam-position for the EDX spectrum given in (B). Copper peaks may result from the use of Cu-grids, but could also be due to an incorporation of copper into greigite magnetosomes (see Pósfai et al., 1998).

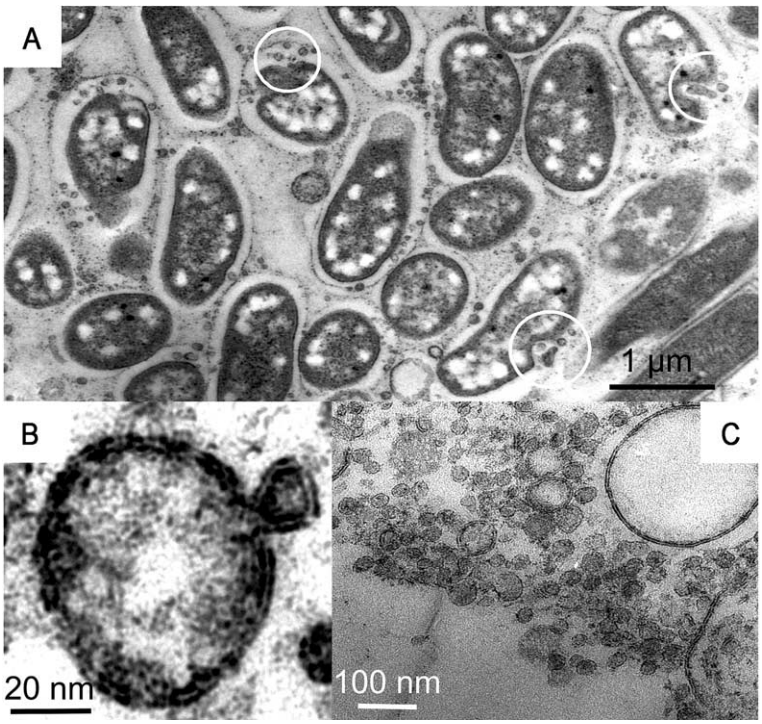

Fig. 8. Putative siderophore vesicles. TEM micrographs. (A) Vesicles in an SRB colony (small spherules clustering in the intercellular space). White circles mark places, where the cell walls of the bacteria invaginate, apparently in order to incorporate these globules. (B) Strong magnification reveals the lipid bilayer of the putative vesicles. This is also a characteristic feature of siderophore vesicles produced by some cultured marine bacteria (e.g. marinobactine; Martinez et al., 2000). (C) A dense cluster of vesicles in an empty ANME-1 sheath. Also note the considerable variation in the size of the vesicles.

et al., 1998; Schüler, 1999). Indeed, FE-SEM/EDX analyses confirmed that the crystallites consist of iron sulphide (Fig. 7). Previous studies showed that the accumulation of intracellular iron sulphides characterises anaerobic magnetotactic bacteria, with ferrimagnetic greigite ($Fe_2^{III}Fe^{II}S_4$) being the principal mineral (Pósfai et al., 1998; Schüler, 1999). It is therefore likely that the iron sulphide aggregates of the Black Sea SRB consist of greigite as well.

3.4. Implications on biogeochemical pathways

Our observations raise questions on the nature of the biogeochemical pathways used by the greigite-forming SRB. Possibly, ferric iron is involved in the oxidation of H_2S (being the product of sulphate-dependant AOM). This could produce ferrous iron contributing to the formation of greigite in the magnetosome chains. Iron reduction, with an energy yield strongly exceeding that of sulphate reduction, may also serve as an additional energy source (cf., Peckmann and Thiel, 2004). However, ferric iron shows an extremely low solubility in marine waters. Some marine bacteria overcome iron shortage by synthesizing extracellular enzymes known as 'siderophores'. Some of these substances consist of a peptidic headgroup with a fatty acyl appendage, and are excreted as micells that scavenge reactive iron in the extracellular environment (Martinez et al., 2000, 2003). Upon iron uptake, the micells re-organize to form larger vesicles which are transferred back into the cells due to their strong membrane affinity. Remarkably, vesicle-like, globular structures are present in the mat surrounding the carbonate concretion (Fig. 8A–C). They are ~20 to 100 nm in diameter and are surrounded by a lipid bilayer structure (Fig. 8B, C), thus matching the size range and organization of siderophore vesicles observed during laboratory experiments with *Marinobacter* sp. ('marinobactin', Martinez et al., 2000). Indeed, cell walls of concretion-associated SRB frequently invaginate upon contact with the globules and it seems as if they are deliberately transferred into the cells (Fig. 8A). Further studies are planned to test whether these structures represent siderophores in their vesicle stage, responsible for the iron acquisition of the greigite-forming SRB, and to identify the source of ferric iron in the reducing environment of the Black Sea seeps.

4. Concluding remarks

Our findings further illustrate a yet unexpected variability of methane-derived carbonates and associated microbes in this permanently anoxic marine environment. Different types of carbonate deposits include highly cavernous towers occurring at sites of free gas venting (not discussed here) and lenticular concretions forming within the sediment. The microbial communities associated with the concretions are different from those of the carbonate towers, revealing a higher biodiversity than previously thought. Although the particular metabolic pathways occurring in the sedimentary environment are still unknown, our data show that the sulphate-dependent AOM is the dominant biogeochemical process that leads to the formation of the concretionary carbonates. The prominent occurrence of greigite-forming, sulphate-reducing bacteria in microbial mats surrounding the concretions also calls the attention to iron cycling as a yet unconsidered process involved in the anaerobic oxidation of methane.

Acknowledgements

We thank the crew of the R/V 'Professor Logachev' for excellent collaboration during the cruise and Martin Ischebek for the on-board fixation of biological samples. Dr. M. Joachimski (Erlangen) is greatly acknowledged for the analyses of stable carbon isotopes. This study received financial support through the project GHOSTDABS (03G0559A) of the Bundesministerium für Bildung und Forschung (BMBF). This is publication GEOTECH-104 of the GEOTECHNOLOGIEN program of the BMBF and the DFG, publication No. 9 of the research project GHOSTDABS, and publication RCOM0233 of the DFG-Research Center for Ocean Margins.

References

Aldrich, H.C., Beimborn, D.B., Schönheit, P., 1987. Creation of internal membranes during fixation of *Methanobacterium thermoautotrophicum*. Can. J. Microbiol. 33, 844–849.

Aloisi, G., Bouloubassi, I., Heijs, S.K., Pancost, R.D., Pierre, C., Sinninghe Damsté, J.S., Gottschal, J.C., Forney, L.J., Rouchy, J.-M., 2002. CH_4-consuming microorganisms and the forma-

tion of carbonate crusts at cold seeps. Earth Planet. Sci. Lett. 203, 195–203.

Amann, R.I., Binder, B.J., Olson, R.J., Chisholm, S.W., Devereux, R., Stahl, D.A., 1990a. Combination of 16S rRNA-targeted oligonucleotide probes with flow cytometry for analyzing mixed microbial populations. Appl. Environ. Microbiol. 56, 1919–1925.

Amann, R.I., Krumholz, L., Stahl, D.A., 1990b. Fluorescent-oligonucleotide probing of whole cells for determinative phylogenetic and environmental studies in microbiology. J. Bacteriol. 172, 762–770.

Blumenberg, M., Seifert, R., Reitner, J., Pape, T., Michaelis, W., 2004. Membrane lipid patterns typify distinct anaerobic methanotrophic consortia. Proc. Natl. Acad. Sci. 101, 11111–11116.

Boetius, A., Ravenschlag, K., Schubert, C.J., Rickert, D., Widdel, F., Gieseke, A., Amann, R., Jørgensen, B.B., Witte, U., Pfannkuche, O., 2000. A marine microbial consortium apparently mediating anaerobic oxidation of methane. Nature 407, 623–626.

Bohrmann, G., Greinert, J., Suess, E., Torres, M., 1998. Authigenic carbonates from the Cascadia subduction zone and their relation to gas hydrate stability. Geology 26, 647–650.

Brown, B.V., 1993. A further chemical alternative to critical-point-drying for preparing small (or large) flies. Fly Times 11, 10.

Campbell, K.A., Farmer, J.D., Des Marais, D., 2002. Ancient hydrocarbon seeps from the Mesozoic convergent margin of California: carbonate geochemistry, fluids and paleoenvironments. Geofluids 2, 63–94.

Chistoserdova, L., Vorholt, J.A., Thauer, R.K., Lidstrom, M.E., 1998. Transfer enzymes and coenzymes linking methylotrophic bacteria and methanogenic archaea. Science 281, 99–102.

Elvert, M., Suess, E., Greinert, J., Whiticar, M.J., 2000. Archaea mediating anaerobic methane oxidation in deep-sea sediments at cold seeps of the eastern Aleutian subduction zone. Org. Geochem. 31, 1175–1187.

Egorov, V.N., Luth, U., Luth, C., Gulin, M.B., 1998. Gas seeps in the submarine Dnieper Canyon, Black Sea: acoustic, video and trawl data. In: Luth, U., Luth, C., Thiel, H. (Eds.), Methane Gas Seep Explorations in the Black Sea (MEGASEEPS), Project Report. Ber. Z. Meeres-u. Klimaforsch, Reihe E 14, Univ. Hamburg, pp. 11–21.

Greinert, J., Bohrmann, J.G., Suess, E., 2001. Gas hydrate-associated carbonates and methane-venting at Hydrate Ridge: classification, distribution, and origin of authigenic lithologies. In: Paull, C.K., Dillon, W.P. (Eds.), Natural Gas Hydrates: Occurrence, Distribution, and Detection, Geophysical Monograph, vol. 124. American Geophysical Union, pp. 87–98.

Hai, T., Lange, D., Rabus, R., Steinbüchel, A., 2004. Polyhydroxyalkanoate (PHA) accumulation in sulfate-reducing bacteria and identification of a class III PHAsynthase (PhaEC) in *Desulfococcus multivorans*. Appl. Environ. Microbiol. 70, 4440–4448.

Hinrichs, K.-U., Boetius, A., 2003. The anaerobic oxidation of methane: new insights in microbial ecology and biogeochemistry. In: Wefer, G., Billet, D., Hebbeln, D., Jørgensen, B.B., Schlüter, M., van Weering, T.C.E. (Eds.), Ocean Margin Systems. Springer, Berlin, pp. 457–477.

Hinrichs, K.-U., Hayes, J.M., Sylva, S.P., Brewer, P.G., DeLong, E.F., 1999. Methane-consuming archaebacteria in marine sediments. Nature 398, 802–805.

Hoffmann, F., Janussen, D., Dröse, W., Arp, G., Reitner, J., 2003. Histological investigation of organisms with hard skeletons: a case study of siliceous sponges. Biotech. Histochem. 78, 191–199.

Ivanov, M.V., Polikarpov, G.G., Lein, A.Y., Galtchenko, V.F., Egorov, V.N., Gulin, S.B., Gulin, M.B., Rusanov, I.I., Miller, Y.M., Kuptsov, V.I., 1991. Biogeochemistry of the carbon cycle in the region of methane gas seeps of the Black Sea. Dokl. Akad. Nauk Ukr. SSR 3205, 1235–1240.

Krüger, M., Meyerdierks, A., Glöckner, F.O., Amann, R., Widdel, F., Kube, M., Reinhardt, R., Kahnt, J., Böcher, R., Thauer, R.K., Shima, S., 2003. A conspicuous nickel protein in microbial mats that oxidize methane anaerobically. Nature 426, 878–881.

Lein, A.Y., Ivanov, M.V., Pimenov, N.V., Gulin, M.B., 2002. Geochemical characteristics of the carbonate constructions formed during microbial oxidation of methane under anaerobic conditions. Microbiology (translated from Mikrobiologiya) 71, 78–90.

Luth, C., Luth, U., Gebruk, A.V., Thiel, H., 1999. Methane gas seeps along the oxic/anoxic gradient in the Black Sea: manifestations, biogenic sediment compounds, and preliminary results on benthic ecology. Pubblicazioni della Stazione Zoologica di Napoli (P.S.Z.N.). Mar. Ecol., Prog. Ser. 20, 221–249.

Manz, W., Eisenbrecher, M., Neu, T.R., Szewzyk, U., 1998. Abundance and spatial organization of Gram negative sulfate-reducing bacteria in activated sludge investigated by in situ probing with specific 16S rRNA targeted oligonucleotides. FEMS Microbiol. Ecol. 25, 43–61.

Manz, W., Arp, G., Schumann-Kindel, G., Szewzyk, U., Reitner, J., 2000. Widefield deconvolution epifluorescence microscopy combined with fluorescence in situ hybridization reveals the spatial arrangement of bacteria in sponge tissue. J. Microbiol. Methods 40, 125–134.

Martinez, J.S., Zhang, G.P., Holt, P.D., Jung, H.-T., Carrano, C.J., Haygood, M.G., Butler, A., 2000. Self-assembling amphiphilic siderophores from marine bacteria. Science 287, 1245–1247.

Martinez, J.S., Carter-Franklin, J.N., Mann, E.L., Martin, J.D., Haygood, M.G., Butler, A., 2003. Structure and membrane affinity of a suite of amphiphilic siderophores produced by a marine bacterium. Proc. Natl. Acad. Sci. 100, 3754–3759.

Michaelis, W., Seifert, R., Nauhaus, K., Treude, T., Thiel, V., Blumenberg, M., Knittel, K., Gieseke, A., Peterknecht, K., Pape, T., Boetius, A., Amann, R., Jørgensen, B.B., Widdel, F., Peckmann, J., Pimenov, N.V., Gulin, M.B., 2002. Microbial reefs in the Black Sea fueled by anaerobic oxidation of methane. Science 297, 1013–1015.

Orphan, V., House, C.H., Hinrichs, K.-U., McKeegan, K.D., DeLong, E.F., 2002. Multiple archaeal groups mediate methane oxidation in anoxic cold seep sediments. Proc. Natl. Acad. Sci. 99, 7663–7668.

Pancost, R.D., Sinninghe Damsté, J.S., 2003. Carbon isotopic compositions of prokaryotic lipids as tracers of carbon cycling in diverse settings. Chem. Geol. 195, 29–58.

Pancost, R.D., Bouloubassi, I., Aloisi, G., Sinninghe Damsté, J.S., the Medinaut Shipboard Scientific Party, 2001. Three series of non-isoprenoidal dialkyl glycerol diethers in cold-seep carbonate crusts. Org. Geochem. 32, 695–707.

Peckmann, J., Thiel, V., 2004. Carbon cycling at ancient methane-seeps. Chem. Geol. 205, 443–467.

Peckmann, J., Reimer, A., Luth, U., Luth, C., Hansen, B.T., Heinicke, C., Hoefs, J., Reitner, J., 2001. Methane-derived carbonates and authigenic pyrite from the northwestern Black Sea. Mar. Geol. 177, 129–150.

Pimenov, N.V., Rusanov, I.I., Poglazova, M.N., Mityushina, L.L., Sorokin, D.Y., Khmelenina, V.N., Trotsenko, Y.A., 1997. Bacterial mats on coral-like structures at methane seeps in the Black Sea. Microbiology (translated from Mikrobiologiya) 66, 354–360.

Pósfai, M., Buseck, P.R., Bazylinsky, D.A., Frankel, R.B., 1998. Iron sulfides from magnetotactic bacteria: structure, composition, and phase transitions. Am. Mineral. 83, 1469–1481.

Reitner, J., 1993. Modern cryptic microbialite/Metazoan facies from Lizard Island (Great Barrier Reef, Australia)—formation and concepts. Facies 29, 3–40.

Reitner, J., Gautret, P., Marin, F., Neuweiler, F., 1995. Automicrites in a modern marine microbialite. Formation model via organic matrices (Lizard Island, Great Barrier Reef, Australia). Bull. Inst. Océanogr. (Monaco) 14, 237–263.

Ritger, S., Carson, B., Suess, E., 1987. Methane-derived authigenic carbonates formed by subduction-induced pore-water expulsion along the Oregon/Washington margin. Geol. Soc. Amer. Bull. 98, 147–156.

Romeis, B., 1989. Mikroskopische Technik. Urban und Schwarzenberg, München.

Schüler, D., 1999. Formation of magnetosomes in magnetotactic bacteria. J. Mol. Microbiol. Biotechnol. 1, 79–86.

Stadnitskaia, A., Baas, M., Ivanov, M.K., van Weering, T.C.E., Sinninghe Damsté, J.S., 2003. Novel archaeal macrocyclic diether core membrane lipids in a methane-derived carbonate crust from a mud volcano in the Sorokin Trough, NE Black Sea. Archaea 1, 165–173.

Thiel, V., Peckmann, J., Richnow, H.H., Luth, U., Reitner, J., Michaelis, W., 2001a. Molecular signals for anaerobic methane oxidation in Black Sea seep carbonates and a microbial mat. Mar. Chem. 73, 97–112.

Thiel, V., Peckmann, J., Schmale, O., Reitner, J., Michaelis, W., 2001b. A new straight-chain hydrocarbon biomarker associated with anaerobic methane cycling. Org. Geochem. 32, 1019–1023.

Tourova, T.P., Kolganova, T.P., Kusnetsov, K.B., Pimenov, N., 2002. Phylogenetic diversity of the Archaeal component of bacterial mats on coral-like structures in zones of methane seeps in the Black Sea. Microbiology (translated from Mikrobiologiya) 71, 196–201.

Valentine, D.L., 2002. Biogeochemistry and microbial ecology of methane oxidation in anoxic environments: a review. Antonie van Leeuwenhook 81, 271–282.

Zeikus, J.G., Wolfe, R.S., 1973. Fine structure of *Methanobacterium thermoautotrophicum*: effect of growth temperature on morphology and ultrastructure. J. Bacteriol. 113, 461–467.